Polaron Ordering in Low-Doping $La_{1-x}Sr_xMnO_3$

Y. Yamada, O. Hino, S. Nohdo, and R. Kanao
Advanced Research Center for Science and Engineering, Waseda University, 3-4-1 Okubo, Shinjuku, Tokyo 169, Japan

T. Inami and S. Katano
Advance Science Research Center, Japan Atomic Energy Research Institute, Tokai, Ibaragi 319-11, Japan
(Received 25 March 1996)

We have found a polaron ordered phase in low-doping rate $La_{1-x}Sr_xMnO_3$ ($x = 0.10$ and 0.15) by neutron scattering study. The onset temperature of the polaron order coincides with the point of resistivity upturn. The periodicity of the hole lattice is commensurate to the structural lattice translation, the unit cell being given by $2a \times 2b \times 4c$ in cubic perovskite basis. The nominal hole concentration corresponding to this periodicity is $n = 0.125$. The polaron lattice seems to have the tendency to lock into this commensurate structure within a finite concentration range around the nominal value of $x = 0.125$. [S0031-9007(96)00669-2]

PACS numbers: 71.38.+i, 61.12.Ex, 64.70.Kb

There has been renewed interest in the properties of the doped Mott insulator $La_{1-x}Sr_xMnO_3$ since it was recognized that the observed "colossal" magnetoresistance could not be explained with a simple double exchange mechanism [1]. Recently, the importance of the role of the electron-phonon interaction has been pointed out [2]. Thus, in addition to spins and conductive holes, we have to take into account the effect of lattice distortion for a full understanding of the physical properties displayed by this material. In this Letter, we focus our attention on the interplay between holes and lattice distortion to understand the relationship between the transport properties and structural properties.

For later convenience, we briefly summarize the structural characteristics of the $La_{1-x}Sr_xMnO_3$ system. It is established that there are two orthorhombic phases (designated as the *O* and *J* phases) and one rhombohedral phase (designated as the *R* phase), each of which is characterized by the type of small distortions from the basic perovskite structure [3]. The distortions are defined by the local vibrational modes of an MnO_6 cluster and its modulation wave vectors with which it propagates through the crystal. The local distortions are composed of the triply degenerated rotational modes (ϕ_x, ϕ_y, ϕ_z) [3–5] and doubly degenerated Jahn-Teller active modes (Q_2, Q_3) [3,6,7]. The structural order parameter of each phase is generally expressed by [8]

$$\Psi(\mathbf{r}) = \sum_i \xi^{(i)} \phi_i e^{i\mathbf{k}_i \cdot \mathbf{r}} + \sum_\nu \eta^{(\nu)} Q_\nu e^{i\mathbf{k}_\nu \cdot \mathbf{r}}, \qquad (1)$$
$$i = x, y, z, \qquad \nu = 2, 3,$$

where $\xi^{(i)}$ and $\eta^{(\nu)}$ are the amplitudes of the relevant modes and $\mathbf{k}_i$ and $\mathbf{k}_\nu$ are the wave vectors. In the upper three columns of Table I, the values of the amplitudes and the corresponding wave vectors for the three phases are listed. Notice that the *J* phase is a "Jahn-Teller ordered" phase because the order parameter includes nonzero amplitudes of Q_2 and Q_3 modes. Upon increasing hole concentration, the three phases successively appear in the order of $J(0 \lesssim x \lesssim 0.1) \rightarrow O(0.1 \lesssim x \lesssim 0.3) \rightarrow R(0.3 \lesssim x)$.

To begin with, we postulate the state of an isolated hole in $LaMnO_3$ to be a small polaron which is given by a localized hole in the $3d(x^2 - y^2)$ orbital surrounded by *inverse* Jahn-Teller distortion. The local distortion is postulated as above because the hole site (Mn^{4+} site) is Jahn-Teller inactive whence the electron-phonon energy is lowered by restoring higher symmetry around the hole.

Therefore, at the high temperature limit, the $La_{1-x}Sr_xMnO_3$ system may be viewed as a polaron liquid, which will eventually transform to a polaron lattice as the temperature is lowered to $T \rightarrow 0$. In fact, formation of hole ordering has been reported in several related materials isomorphous with $LaMnO_3$ [9] and La_2CuO_4 [10,11].

TABLE I. The amplitudes of local vibrational modes and relevant wave vectors which characterize each phase stabilized in the low-doping $La_{1-x}Sr_xMnO_3$ ($0 \le x \le 0.3$). The "*P* phase" given in the last column specifies the newly found polaron ordered phase as given in Eq. (2).

Phase	Amplitude	*K*
R	$\xi^{(x)} = \xi^{(y)} = \xi^{(z)} \neq 0$	1/2 1/2 1/2
	$\eta^{(2)} = \eta^{(3)} = 0$	⋯
O	$\xi^{(x)} = \xi^{(y)} \neq 0$	1/2 1/2 1/2
	$\xi^{(z)} \neq 0$	1/2 1/2 0
	$\eta^{(2)} = \eta^{(3)} = 0$	⋯
J	$\xi^{(x)} = \xi^{(y)} \neq 0$	1/2 1/2 1/2
	$\xi^{(z)} \neq 0$	1/2 1/2 0
	$\eta^{(2)} \neq 0$	1/2 1/2 0
	$\eta^{(3)} \neq 0$	0 0 0
P	$\xi^{(x)} = \xi^{(y)} \neq 0$	1/2 1/2 1/2
	$\xi^{(z)} \neq 0$	1/2 1/2 0
	$\eta^{(2)} \neq 0$	1/2 1/2 1/4
	$\eta^{(3)} = 0$	⋯

 0031-9007/96/77(5)/904(4)$10.00

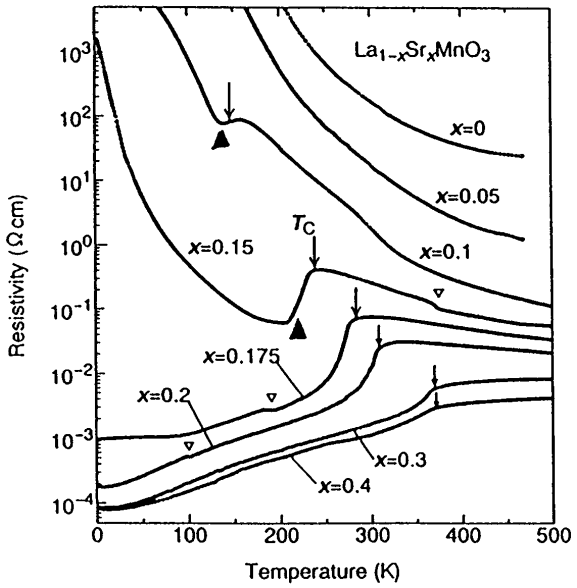

FIG. 1. Temperature dependencies of resistivity of $La_{1-x}Sr_xMnO_3$ at various values of the doping rate x. Arrows indicate the ferromagnetic transition points. Triangles indicate the points of resistivity upturn which are observed in the range of $0.1 \leq x \leq 0.15$. Figure is taken from Ref. [12].

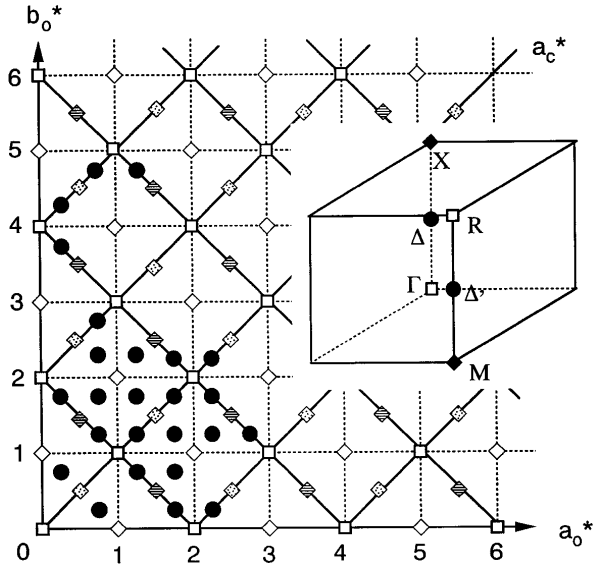

FIG. 2. Schematic representation of the observed diffraction pattern. The solid lines represent the pseudocubic $(h,k,0)_c$ reciprocal lattice. The dashed lines give the orthorhombic $(h,k,0)_o$ lattice. The small solid circles give the positions of the newly found satellites. The inset shows the corresponding positions of the Bragg reflections in the first Brillouin zone of pseudocubic reciprocal space. Notice Δ and Δ' points are equivalent when referred to the exact orthorhombic symmetry. The equivalent superlattice reflections originating from the different domains are distinguished by the following symbols: open diamond M points of domain I; striped diamond X points of domain II; dotted diamond X points of domain III.

In this connection, we take notice of the anomalous behavior in resistivity curves [12] in $La_{1-x}Sr_xMnO_3$ with $0.1 \lesssim x \lesssim 0.16$ (see Fig. 1). As clearly seen in the case of $x = 0.15$, the resistivity suddenly decreases at the ferromagnetic Curie point $T_c = 240$ K, indicating the onset of a "metallic" phase, then it starts to increase again at $T \approx 190$ K. Similar behavior is also seen in the case of $x = 0.10$ though the anomaly is less conspicuous. It would be reasonable to identify the point of resistivity upturn to be the onset point of polaron lattice formation, where holes start to freeze on the lattice sites. From this view point, the $La_{1-x}Sr_xMnO_3$ system with $0.1 < x < 0.16$ is considered to undergo successive transition as polaron liquid (insulator) $\rightarrow$ Fermi liquid ("metal") $\rightarrow$ polaron lattice (insulator).

In order to verify these considerations, we have carried out neutron scattering experiments on the samples of $x = 0.10$ and $x = 0.15$. Standard type triple axis neutron spectrometers installed at the JRR-3M reactor in the Japan Atomic Energy Research Institute were utilized. Crystals are grown by floating zone melting technique, the details described elsewhere [12]. The as-grown crystals are pseudocubic single crystals with 20 mm $\times$ 4 mm inner diam in size, which are composed of domains of microtwins of the true orthorhombic lattices. The mosaic spread within a single domain is less than 0.8°. Beam collimation was 40′ and 40′ before and after the sample position. Crystals are mounted on an aluminum rod and covered by an aluminum container filled with He gas to ensure thermal equilibrium. The temperature of the container was controlled within 0.1 K. The preliminary observations confirm that the sample with $x = 0.15$ is in the O phase, while, in contrast, the sample with $x = 0.10$ is the J phase at room temperature.

We carried out fine mesh scans at $T = 10$ K over a wide region in the $(h,k,0)_c$ reciprocal space, with a step of $\delta h, \delta k = 0.05 a_0^*$. For both samples with $x = 0.10$ and $x = 0.15$, we find a series of satellite reflections as schematically shown in Fig. 2. The satellite positions are apparently indexed as $(h \pm 1/4,\ k \pm 1/4,\ 0)_o$. However, since the samples are multidomain crystals composed of microtwins, there is another possible indexing referring to the true orthorhombic lattice: $(h,k,l \pm 1/2)_o$. (Both are equivalent positions when referred to the pseudocubic reciprocal space.) In order to distinguish these two possibilities electron diffraction observations are carried out using single domain samples. It turns out that the true index is $(h,k,l \pm 1/2)_o$ [13]. The positions of Bragg reflections within the pseudocubic Brillouin zone are depicted in the inset of Fig. 2. The main Bragg reflections due to the average perovskite structure appear at Γ points. The superlattice reflections due to the small distortions at M or X points, and the newly observed satellites are at Δ and Δ' points.

Temperature dependencies of the satellite intensities as well as the main Bragg reflections (Γ points) and the superlattice reflections (X or M points) are investigated. The results are summarized in Fig. 3. We notice the

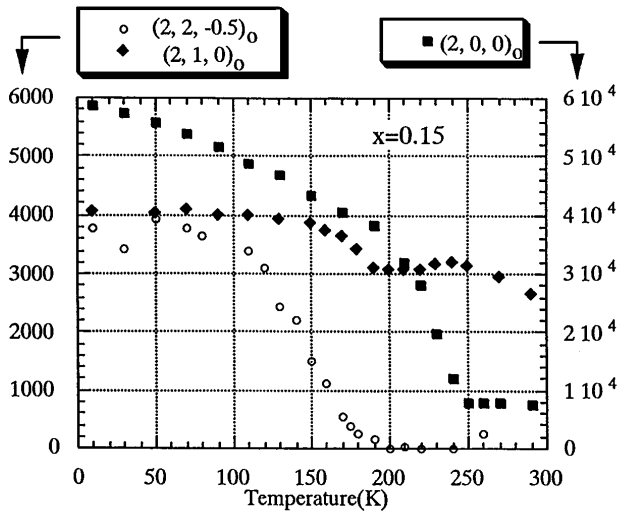

(a)

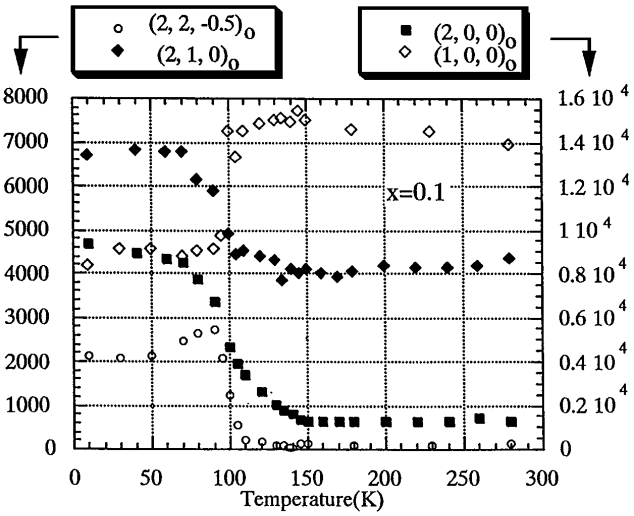

(b)

FIG. 3. Temperature dependencies of the intensities of various types of reflections: (a) $x = 0.15$, (b) $x = 0.10$. The important characteristics of each type of reflection for both cases are described in the text.

following important characteristics of the experimental results.

Figure 3(a) (the results on the sample with $x = 0.15$).—(i) The satellite reflection $(2, 2, -0.5)_o$ sets in at $T_p = 190$ K, exactly corresponding to the point of resistivity upturn. (ii) The main Bragg reflection $(2, 0, 0)_o$ starts to increase at $T_c = 240$ K corresponding to the onset of ferromagnetic order. (iii) The superlattice reflection $(2, 1, 0)_o$ shows a break at T_p and increases below T_p. (iv) Temperature variation of the satellite and the superlattice reflections at $T \leq T_p$ is rather gradual indicating that the transition at T_p is of second order type.

Figure 3(b) (the results on the sample with $x = 0.10$).—(v) The satellite reflection $(2, 2, -0.5)_o$ sets in at $T_p \approx 100$ K, where the resistivity curve shows similar upturn. (vi) The main Bragg reflection $(2, 2, 0)_o$ starts to increase at $T_N \approx 120$ K, corresponding to the onset of a ferromagnetic component of magnetic order. (vii) The superlattice reflection $(1, 0, 0)_o$ shows an abrupt decrease at T_p. (viii) Temperature variation of the satellite and superlattice reflections shows clear cutoff indicating that the transition at T_p is of first order type.

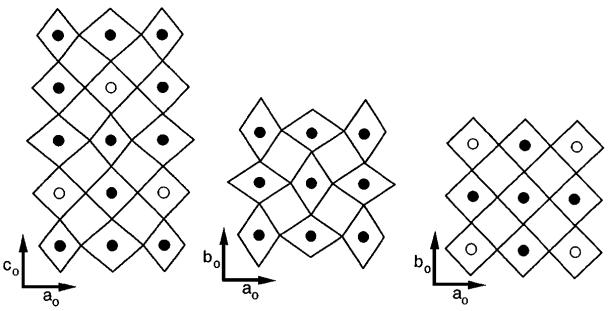

FIG. 4. The observed structure in the *P* phase as given by Eq. (2). The hole site (Mn^{4+} site) is indicated by the open circle. The atomic configuration in the first and third layers is identical with those of the *J* phase. The second and fourth layers which include holes recover higher symmetry equivalent to the *O* phase.

These experimental results are consistently explained by the following picture: The transition at T_p is due to the polaron ordering. The lattice distortion in the polaron ordered phase (designated as "*P* phase" hereafter) is characterized by the order parameter

$$\Psi^{(P)}(\mathbf{r}) = \Psi^{(O)}(\mathbf{r}) + \eta O_2 e^{i\mathbf{k}_2^{(P)}\cdot\mathbf{r}}, \qquad (2)$$

$$\mathbf{k}_2^{(P)} = (1/2, 1/2, 1/4),$$

where $\Psi^{(O)}(r)$ is the order parameter of the *O* phase. The actual distortion pattern given by Eq. (2) and the

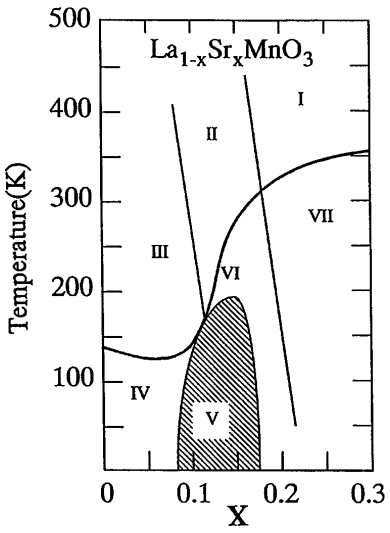

FIG. 5. The overall phase diagram with respect to doping rate *x* and temperature *T*. The magnetic phase boundary is taken from Ref. [12]. The shaded region is the newly found polaron ordered phase. The physical properties associated with structure, magnetism, and hole transport in each phase are summarized in Table II.

TABLE II. The physical properties of each phase specified in Fig. 5. Phase *V* is the polaron ordered phase. The magnetic structure in *P* phase is not established.

	I	II	III	IV	V	VI	VII
magnetic	Para	Para	Para	AF	(Ferri)	F	F
transport	I	I	I	I	I	M	M
structure	R	O	J	J	P	O	R

Para: paramagnetic
AF: antiferromagnetic
F: ferromagnetic
Ferri: ferrimagnetic
I: insulator
M: metal
R: rhombohedral
O: orthorhombic (J-T disordered)
J: orthorhombic (J-T ordered)
P: orthorhombic (polaron ordered)

associated hole ordering is depicted in Fig. 4, in which the rotational distortions are neglected for simplicity. We see that the atomic arrangement in one of the successive two layers is identical with that of the Jahn-Teller (JT) ordered *J* phase, while the other layer which contains holes recovers higher symmetry similar to the JT disordered *O* phase. The recovery is caused by the postulated inverse JT distortion around the holes. As is seen in the figure, holes in the latter layer construct 2×2 square lattice referring to the cubic perovskite unit. Therefore, the hole concentration is $n = 1/2 \times 1/2 \times 1/2 = 0.125$, which means that the hole lattice in Fig. 4 is exactly constructed at the nominal doping rate of $x = 0.125$, just in between the x values investigated. It seems that the commensurate polaron order as given in Fig. 4 is so strongly stabilized that the polaron ordering tends to lock into this commensurate structure even when the x value is slightly off from the "stoichiometric value" of $x = 0.125$. The excess (or deficient) holes due to off-stoichiometry should leave some disordering concerning hole configuration. In fact, we observe strong diffuse scattering even at 10 K around main Bragg reflections in both samples of $x = 0.10$ and $x = 0.15$.

As for the order of the phase transition we notice that the transition from the *O* phase to *P* phase is a disorder-order transition in terms of the JT ordering, while the transition from *J* phase to *P* phase is that from an ordered phase [specified by the wave vector $\mathbf{k} = (1/2, 1/2, 0)$] to another ordered phase [specified by the wave vector $\mathbf{k} = (1/2, 1/2, 1/4)$]. This is consistent with the observed characteristics described in (iv) and (viii).

It is instructive to look upon the *P* phase as a "partially ordered" state concerning JT ordering since it is composed of alternation of the perfectly JT ordered layers and the undistorted layers. From this view point, the experimental results described in (iii) and (vii) are naturally understood: The *O*-*P* transition corresponds to a partial increase of JT order while the *J*-*P* transition is viewed as a partial decrease of the complete JT order.

To complete Table I, we add the last column specifying the newly found "polaron ordered" phase. Together with the previously known magnetic phase diagram [12], we can construct the overall phase diagram somewhat schematically as given in Fig. 5. The characteristics of each phase associated with magnetism, conductivity, and structure are listed in Table II. The magnetic structure in phase *V* (*P* phase) is not established. We simply assume that it would be ferrimagnetic phase since it is intervening between the *A*-type antiferromagnetic phase of pure $LaMnO_3$ and the ferromagnetic phase of highly doped $LaSrMnO_3$.

We wish to thank Professor Y. Tokura of the University of Tokyo and Dr. Moritomo of the Joint Research Center for Atom Technology for providing us excellent single crystals for neutron scattering experiment. We further acknowledge Professor M. Tachiki for valuable discussions. This work has been partly supported by ISSP for using the neutron spectrometer installed at JRR-3 reactor in Japan Atomic Energy Research Institute.

[1] A. J. Millis, P. B. Littlewood, and B. I. Shraiman, Phys. Rev. Lett. **74**, 5144 (1995).
[2] A. J. Millis, B. I. Shraiman, and R. Mueller (unpublished).
[3] A. K. Bogush, V. I. Pavlov, and L. V. Balyko, Cryst. Res. Technol. **18**, 589 (1983).
[4] M. A. Gilleo, Acta Cryst. **10**, 161 (1957).
[5] J. B. A. A. Ellemans, B. van Laar, K. R. van der Veen, and B. O. Loopstra, J. Solid State Chem. **3**, 238 (1971).
[6] J. Kanamori, J. Appl. Phys. Suppl. **31**, 14S (1960).
[7] G. Matsumoto, J. Phys. Soc. Japn. **29**, 606 (1970).
[8] Y. Fujii, S. Hoshino, Y. Yamada, and G. Shirane, Phys. Rev. B **9**, 4549 (1974).
[9] Z. Jirak, S. Krupicka, V. Nekvasil, E. Pollert, G. Villeneuve, and F. Zounova, J. Magn. Magn. Mater. **15–18**, 519 (1980).
[10] J. M. Tranquada, B. J. Sternlleb, J. D. Axe, Y. Nakamura, and S. Uchida, Nature (London) **375**, 561 (1995).
[11] C. H. Chen, S-W. Cheong, and A. S. Cooper, Phys. Rev. Lett. **71**, 2461 (1993).
[12] A. Urushibara, Y. Moritomo, T. Arima, A. Asamitsu, G. Kido, and Y. Tokura, Phys. Rev. B **51**, 14 103 (1995).
[13] S. Mori (private communication).